

Electronic thermal conductivity at high temperatures: Violation of the Wiedemann-Franz law in narrow band metals

K. Vafayi,¹ M. Calandra,² and O. Gunnarsson¹

¹*Max-Planck-Institut für Festkörperforschung, D-70506 Stuttgart, Germany and*

²*Institut de Minéralogie et de Physique des Milieux Condensés, 4 place Jussieu, 75252, Paris cedex 05, France*

We study the electronic part of the thermal conductivity κ of metals. We present two methods for calculating κ , a quantum Monte-Carlo (QMC) method and a method where the phonons but not the electrons are treated semiclassically (SC). We compare the two methods for a model of alkali-doped C₆₀, A₃C₆₀, and show that they agree well. We then mainly use the SC method, which is simpler and easier to interpret. We perform SC calculations for Nb for large temperatures T and find that κ increases with T as $\kappa(T) = a + bT$, where a and b are constants, consistent with a saturation of the mean free path, l , and in good agreement with experiment. In contrast, we find that for A₃C₆₀, $\kappa(T)$ decreases with T for very large T . We discuss the reason for this qualitatively in the limit of large T . We give a quantum-mechanical explanation of the saturation of l for Nb and derive the Wiedemann-Franz law in the limit of $T \ll W$, where W is the band width. In contrast, due to the small W of A₃C₆₀, the assumption $T \ll W$ can be violated. We show that this leads to $\kappa(T) \sim T^{-3/2}$ for very large T and a strong violation of the Wiedemann-Franz law.

I. INTRODUCTION

In the Sommerfeld theory, the electronic contribution κ to the thermal conductivity of a metal can be written as¹

$$\kappa = \frac{1}{3} v_F l c_v = \frac{\pi^2}{3} \frac{n k_B^2}{m v_F} l T, \quad (1)$$

where v_F is the Fermi velocity, l the mean free path, $c_v = \pi^2 k_B^2 n T / (m v_F^2)$ is the specific heat per electron, n is the electron density, k_B is the Boltzmann constant, m is the electron mass and T the temperature. For large T the mean free path decreases as $l \sim 1/T$, and one might then expect that κ approximately approaches a constant for large T . This is indeed found for many good metals. However, in the context of electrical conductivity, it has been found that for large T the so-called parallel resistor formula describes the experimental resistivity quite well for many metals with a large resistivity.² This formula corresponds to the assumption

$$l = d + \frac{c}{T}, \quad (2)$$

where d is a distance of the order of the separation of two atoms and c is a constant. According to this formula the mean free path initially decreases rapidly with T but then saturates at $l \sim d$. This formula is often justified by arguing that in a semiclassical picture, at worst, an electron is scattered at every atom, leading to $l \sim d$. Inserting Eq. (2) in Eq. (1) leads to

$$\kappa = a + bT, \quad (3)$$

where a and b are constants. This formula gives a fairly good qualitative description of experimental results for many transition metal and transition metal compounds with a small κ .

The theoretical justification for Eq. (2), however, is very unsatisfactory. It is based on a semiclassical picture, which is only valid for $l \gg d$, and which cannot be

used to discuss what happens for $l \sim d$. Nevertheless, in the 1970's and early 1980's it seemed that $l \gtrsim d$ was a universal behavior,³ satisfying the Ioffe-Regel condition.⁴ Later experimental work, however, has found many examples of metals where the resistivity is much larger than predicted by the Ioffe-Regel condition and where the apparent mean free path is much shorter than the separation of two atoms.⁵ This illustrates that the semiclassical explanation for Eq. (2) is incorrect and there is a need for a quantum-mechanical explanation of Eq. (3). Such a theory has been presented in the context of the electrical conductivity.⁶ The purpose of this paper is to provide a quantum-mechanical justification for the thermal conductivity in Eq. (3).

To calculate the thermal conductivity we use a Quantum Monte-Carlo (QMC) method, which can solve the models used here accurately. To interpret the results, we also introduce a simpler semiclassical (SC) method, where the phonons but not the electrons are treated semiclassically.

For many metals, the Wiedemann-Franz law

$$\frac{\kappa}{\sigma T} = \frac{\pi^2}{3} \left(\frac{k_B}{e} \right)^2, \quad (4)$$

is approximately satisfied, where σ is the electrical conductivity and e the electron charge. We derive this law by making assumptions which are expected to be reasonable when T is so large that the transport is completely incoherent but T is still much smaller than W , where W is the band width. For $T \gtrsim W$, however, we find that the Wiedemann-Franz law is strongly violated. This may apply to alkali-doped fullerenes, A₃C₆₀, at or somewhat above the highest temperatures that can be achieved experimentally.

In Sec. II we present the models and in Sec. III the methods used. In Sec. IV we compare the QMC and SC methods. The results for Nb and A₃C₆₀ in the SC method are given in Sec. V. These results are discussed qualitatively in Sec. VI.

II. MODELS

We first consider a model of Nb, referred to as the transition metal (TM) model, which is appropriate for describing transition metals or transition metal compounds. Each Nb atom has a five-fold degenerate ($N_d = 5$) level. The hopping matrix elements are described by $t_{\mu\nu}$, where $\nu \equiv (m, i)$ is a combined label for a orbital index m and a site index i . Thus the electronic Hamiltonian is

$$H_0^{\text{el}} = \varepsilon_0 \sum_{\mu\sigma} c_{\mu\sigma}^\dagger c_{\mu\sigma} + \sum_{\mu\nu\sigma} t_{\mu\nu} c_{\mu\sigma}^\dagger c_{\nu\sigma}, \quad (5)$$

where $c_{\mu\sigma}^\dagger$ creates an electron in the state μ with spin σ . We assume that the Coulomb interaction can be neglected, since the band width of Nb is rather large. The precise form of the hopping matrix elements has been described elsewhere.⁷

We assume that the electron scattering is due to the electron-phonon coupling. For the Nb model, we assume that the phonons couple to hopping integrals (HI). The phonons are approximated as Einstein phonons, with one phonon for each coordinate direction. The frequency $\omega_{ph} = 0.014$ eV was set equal to the average phonon frequency of Nb metal.⁸ Due to the vibrations of the atoms the hopping matrix elements are modulated, leading to an electron-phonon coupling.⁷

We next introduce a model of alkali-doped C_{60} , A_3C_{60} , referred to as the C_{60} model. We use a model including the partly occupied three-fold degenerate t_{1u} orbital on each C_{60} and the hopping matrix elements connecting these orbitals. This results in a Hamiltonian of the same general form as in Eq. (5) but with a different lattice structure and different orbital degeneracy ($N_d = 3$). The hopping integrals are obtained from a tight-binding description.^{7,9} For simplicity, the Coulomb interaction is neglected, although this may be a questionable approximation. The main electron-phonon coupling is due to the intramolecular five-fold degenerate phonons of H_g symmetry, which have an on-site Jahn-Teller coupling to the t_{1u} levels of a C_{60} molecule.^{7,9} We refer to this as a level energy (LE) coupling. For the TM and C_{60} models we define the dimensionless coupling λ so that the real part of the electron-phonon part of the electron self-energy is given by

$$\text{Re}\Sigma_{\text{ep}}(\omega) = -\lambda\omega, \quad (6)$$

in the weak-coupling limit and for small ω .

To introduce current operators we follow Mahan.¹⁰ The particle current is obtained from particle conservation

$$\mathbf{j} = \frac{i}{\hbar} [H, \mathbf{P}] = -\frac{i}{\hbar} \sum_{\mu\nu\sigma} (\mathbf{R}_\mu - \mathbf{R}_\nu) t_{\mu\nu} c_{\mu\sigma}^\dagger c_{\nu\sigma}, \quad (7)$$

where H is the full Hamiltonian and \mathbf{P} is the polarization operator

$$\mathbf{P} = \sum_i \mathbf{R}_i n_i. \quad (8)$$

Here $\mathbf{R}_\nu = \mathbf{R}_i$ is the position of the i th atom ($\nu = (m, i)$). In a similar way the energy current is obtained from energy conservation

$$\begin{aligned} \mathbf{j}_E &= \frac{i}{\hbar} \sum_i \mathbf{R}_i [H, h_i] \\ &= -\frac{i}{2\hbar} \sum_{\mu\gamma\nu\sigma} t_{\mu\gamma} t_{\gamma\nu} (\mathbf{R}_\mu - \mathbf{R}_\nu) c_{\mu\sigma}^\dagger c_{\nu\sigma}, \end{aligned} \quad (9)$$

where h_i is a Hamiltonian of the i th atomic site, defined in such a way that the hopping terms between two sites are split equally between these two sites and $H = \sum_i h_i$. Following Ref. 10, we also introduce a heat current

$$\mathbf{j}_Q = \mathbf{j}_E - \mu \mathbf{j}, \quad (10)$$

where μ is the chemical potential.

III. METHODS

The conductivity is calculated using a Kubo formalism. We assume an isotropic system and define a heat current - heat current correlation function¹⁰

$$\pi^{(22)}(i\omega_n) = -\frac{1}{3N\Omega} \int_0^{\beta\hbar} d\tau e^{i\omega_n\tau} \langle T_\tau \mathbf{j}_Q(\tau) \cdot \mathbf{j}_Q(0) \rangle, \quad (11)$$

where N is the number of atoms, Ω is the volume per atom, $\beta = 1/(k_B T)$, T_τ is a time-ordering operator and ω_n is a Matsubara frequency. In a similar way we define a particle current - heat current correlation function $\pi^{(12)}$ and a particle current - particle current correlation function $\pi^{(11)}$. These correlation functions are analytically continued, giving retarded response functions $\pi_{\text{ret}}^{nm}(\omega)$. Then the electrical conductivity is given by¹⁰

$$\sigma(\omega) = -e^2 \frac{\text{Im}\pi_{\text{ret}}^{(11)}(\omega)}{\hbar\omega}. \quad (12)$$

The heat conductivity is¹⁰

$$\kappa(\omega) = -\frac{1}{T\hbar\omega} \left\{ \text{Im}\pi_{\text{ret}}^{(22)}(\omega) - \frac{[\text{Im}\pi_{\text{ret}}^{(12)}(\omega)]^2}{\text{Im}\pi_{\text{ret}}^{(11)}(\omega)} \right\}. \quad (13)$$

We use two different methods for performing calculations, a determinantal quantum Monte-Carlo (QMC) method¹¹ and a semiclassical (SC) method. The QMC method can be used to obtain properties very accurately. To interpret these results we use a SC method where the phonons but not the electrons are treated semiclassically.

Due to the lack of a repulsive Coulomb interaction in the models treated here, the QMC method has no so-called sign problem. The statistical errors in the QMC calculation of response functions for imaginary times can then be made arbitrarily small by improving the sampling. To analytically continue these response functions to the real frequency axis we use a maximum entropy method.¹²

The Hamiltonians treated here can be written in the form

$$\begin{aligned} H &= H_0^{\text{el}} + \sum_{\mu\nu n\sigma} g_{\mu\nu n} c_{\mu\sigma}^\dagger c_{\nu\sigma} q_n + \frac{1}{2} \sum_n (p_n^2 + \omega_{\text{ph}}^2 q_n^2) \\ &\equiv H^{\text{el}}(\mathbf{q}) + H_B, \end{aligned} \quad (14)$$

where $g_{\mu\nu n}$ is a coupling constant, q_n is a phonon coordinate, p_n a phonon momentum and ω_{ph} is the frequency of the phonons. In the QMC calculation the starting point is the partition function

$$Z = \text{Tr} \int d\mathbf{q} \langle \mathbf{q} | e^{-\beta H} | \mathbf{q} \rangle \quad (15)$$

where Tr is a trace over all electronic states and the integral over $\mathbf{q} \equiv (q_1, q_2, \dots)$ results in a trace over \mathbf{q} . Since $H^{\text{el}}(\mathbf{q})$ and H_B do not commute, we use a Trotter decomposition and define $\Delta\tau = \beta\hbar/L$, where L is some integer. We write $\exp(-\beta H)$ as $\prod_{i=1}^L \exp(-\Delta\tau H_{\text{el}}(\mathbf{q})) \exp(-\Delta\tau H_B)$. By inserting complete sets of phonon states between each factor, one obtains^{11,13}

$$\begin{aligned} Z &= \text{Tr} \int (\prod_{i=1}^L d\mathbf{q}_i) e^{-\Delta\tau H_{\text{el}}(\mathbf{q}_1)} \langle \mathbf{q}_1 | e^{-\Delta\tau H_B} | \mathbf{q}_L \rangle \\ &\times \dots e^{-\Delta\tau H_{\text{el}}(\mathbf{q}_2)} \langle \mathbf{q}_2 | e^{-\Delta\tau H_B} | \mathbf{q}_1 \rangle \end{aligned} \quad (16)$$

The phonon coordinates $\mathbf{q}_i \equiv \{q_{n,i}\} \equiv \{q_n(\tau_i)\}$ are sampled by using a Monte-Carlo approach with the integrand as a weight factor. Here $\tau_i = i\Delta\tau$ is an imaginary time. Correlation functions $\langle X(\tau_i) X(\tau_j) \rangle$ are obtained in a similar way by inserting the operators at positions corresponding to τ_i and τ_j .^{11,13} For the case of the HI coupling there are technical complications in terms of updating the relevant quantities after each Monte-Carlo step, which are discussed elsewhere.⁷

In the SC treatment of the phonons,⁷ we introduce a super cell with periodic boundary conditions. Each phonon coordinate is given a random displacement according to a Gaussian distribution centered at zero and with the width

$$\langle x^2 \rangle = \frac{\hbar}{M\omega_{\text{ph}}} [n_B(T) + 0.5] \quad (17)$$

where

$$n_B(T) = \frac{1}{e^{\hbar\omega_{\text{ph}}/(k_B T)} - 1}, \quad (18)$$

is the occupation of the phonon mode. For fixed phonon coordinates, the resulting Hamiltonian is a one-particle Hamiltonian, which can easily be diagonalized. The response functions $\pi^{(nm)}$ can then be expressed in terms of the eigenstates $|l\rangle$ and eigenvalues ε_l of this Hamiltonian as

$$\begin{aligned} \text{Im}\pi_{xx}^{(mn)}(\omega) &= -\frac{2\pi\hbar}{N\Omega} \sum_{l'l'} \langle l | (j_m)_x | l' \rangle \langle l' | (j_n)_x | l \rangle \\ &\times (f_l - f_{l'}) \delta(\hbar\omega + \varepsilon_l - \varepsilon_{l'}), \end{aligned} \quad (19)$$

where $j_1 = j$, $j_2 = j_Q$ and f_l is the Fermi function for the energy ε_l . We have here for simplicity considered the xx component. The result is averaged over different configurations of random displacements of the atoms.

The electron-phonon interaction leads to a renormalization of the phonon frequency. This renormalization acts back on the electronic properties. This is included in the QMC approach above, but not in the SC method. To be able to compare more directly with this SC method, we also perform QMC calculations where the electron-phonon interaction is neglected when calculating the weight functions entering the sampling in Eq. (16). In all other parts of the QMC calculation the electron-phonon interaction is fully taken into account. The result is that the phonon coordinates are sampled as if the phonons were free phonons. In *this* QMC calculation, the phonons are then not renormalized, and the corresponding influence on the electronic properties is absent.

IV. COMPARISON OF QMC AND SEMICLASSICAL METHODS

To test the accuracy of the SC method, we compare the thermal conductivity of the C₆₀ model according to the QMC and SC method. As discussed in Sec. III, in the QMC calculation the phonon frequency is renormalized by the electron-phonon interaction, while this is not the case in the SC calculation. To compare the two methods we use two different approaches. In one approach we suppress the phonon renormalization in the QMC calculation, as discussed in Sec. III. In a second approach we calculate an effective phonon frequency, ω_{eff} , in the QMC program and then put in this frequency by hand in the SC calculation, keeping the coupling constants fixed. To obtain the effective phonon frequency we calculate the phonon Green's function $D(\tau)$ for imaginary times τ . We compare this with the phonon Green's function, $D_0(\tau, \omega_{\text{eff}})$, for noninteracting phonons with the frequency ω_{eff} . We minimize

$$\sum_i [D(\tau_i) - D_0(\tau_i, \omega_{\text{eff}})]^2 \quad (20)$$

with respect to ω_{eff} , where τ_i correspond to the discrete values of τ used in the QMC calculation. The electron-phonon coupling constants are kept unchanged.

In the SC method $\kappa(\omega)$ is calculated directly for real frequencies, while in the QMC method we calculate the response functions $\pi^{nm}(\tau)$ for imaginary times and then use a maximum entropy method (MEM) to perform the analytical continuation. To make the QMC and SC methods more comparable, we have therefore in the SC method also made a transformation of the data to imaginary times for each random configuration, which is an accurate and well-behaved transformation. We have then transformed the data back to real frequencies, using MEM. These results, referred to as SCMEM results,

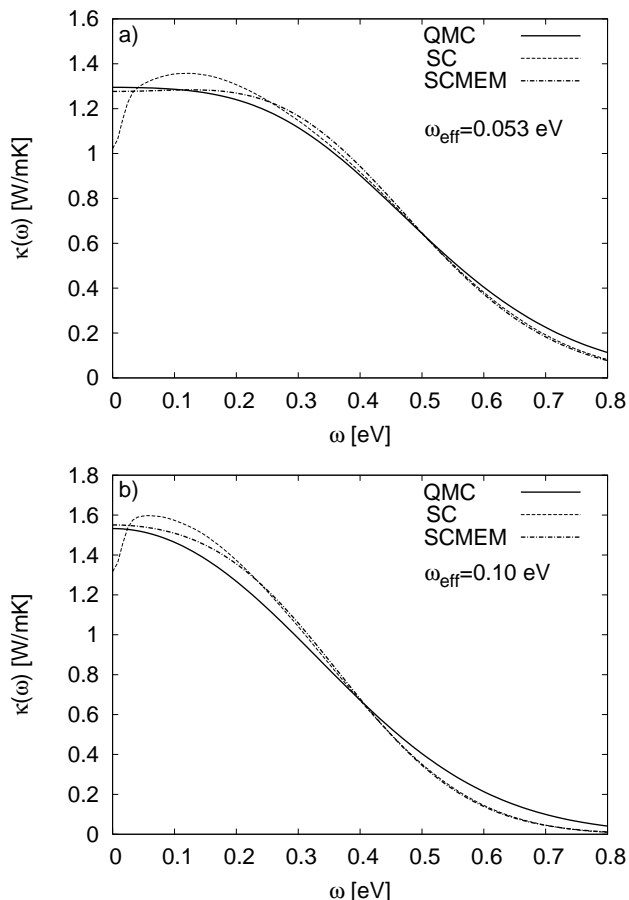


FIG. 1: a) Thermal conductivity $\kappa(\omega)$ of A_3C_{60} as a function of ω according to QMC (full line), SC (dashed line) and SCMEM (dashed-dotted line). b) The same as in a) but with the renormalization of the phonon frequency suppressed. The parameters are $\omega_{ph} = 0.1$ eV, $\lambda = 0.5$ and $T = 0.1$ eV. In a) ω_{ph} is renormalized to $\omega_{\text{eff}} = 0.053$ eV. The model of A_3C_{60} described in Sec. II was used. The calculations were done for a cluster with $3 \times 4 \times 4$ sites and averaged over 20000 different random configurations. A Gaussian broadening with FWHM 0.03 eV was used. The figure illustrates that the QMC and SCMEM calculations agree very well and that the downturn at $\omega = 0$ in the SC results is lost in the SCMEM results due to the MEM procedure.

then contain errors introduced by the analytical continuation, and are in this sense more comparable to the QMC results.

Fig. 1 shows results for $\kappa(\omega)$ of the C_{60} model for $T = 0.1$ eV, $\omega_{ph} = 0.1$ eV and $\lambda = 0.5$. In the QMC calculation the phonon frequency is renormalized to $\omega_{\text{eff}} = 0.053$ eV. In Fig. 1a the phonon renormalization is taken into account and in Fig. 1b it is suppressed. It is interesting that the QMC and SCMEM data agree quite well, both with and without renormalization of the phonon frequency. This suggests that the SC method is rather accurate. We also notice that the renormalization of the phonon frequency leads to an effectively stronger electron-phonon coupling and therefore

a smaller $\kappa(\omega = 0)$. This follows since the coupling goes as the inverse phonon frequency if the coupling constants are kept fixed, as is done here.

The SC results show a downturn for small ω . This may be the beginning of an Anderson localization.¹⁴ In the SC method, the phonons introduce a static (diagonal) disorder which leads to an Anderson localization when the disorder becomes sufficiently strong. This is not expected to happen in the QMC calculation, since this calculation takes into account that the scattering is inelastic and phase information is lost.¹⁴ We note, however, that if such a downturn actually would occur in the QMC spectrum, it would be lost in the analytical continuation to real frequencies. This can be seen by comparing the SC and SCMEM curves, since the downturn in the SC results is lost in the SCMEM results, due to the MEM procedure. The reason is that the downturn happens on such a small energy scale that it is not detected by the MEM.

Since there is a rather good agreement between the QMC and SC methods, we use the SC method in the rest of the paper. The reason is that the SC method is simpler, and it is easier to interpret the results.

V. RESULTS USING THE SEMICLASSICAL METHOD

We have calculated the thermal conductivity of Nb using the SC method. We used a cluster of $10 \times 10 \times 10$ atoms and averaged over 10 different distributions of thermally displaced atoms. The model described in Sec. II was used. The results are compared with experimental results^{16,17,18,19} in Fig. 2. Theory and experiment agree rather well. The figure also shows the curve $\kappa(T) = (47.5 + 0.013T)$ W/mK fitted to the experimental results. This linear dependence on T is in qualitative agreement with the result expected from the discussion in Sec. VI below. $\kappa(T)$ increases with T , which within the framework of the discussion in the introduction would correspond to the saturation of the apparent mean free path [see Eq. (3)].

The thermal conductivity of A_3C_{60} was calculated using the SC method for a cluster of $8 \times 8 \times 8$ molecules and averaging over 400 different distributions of thermally distorted molecules. The parameters were $\lambda = 0.5$ and $\omega_{ph} = 0.1$ eV, where $\omega_{ph} = 0.1$ eV is an approximate average renormalized phonon frequency for A_3C_{60} . The results are shown in Fig. 3. The results are influenced by a downturn for small ω (see Fig. 1), which depends on the amount of broadening used. For the temperatures shown in Fig. 3 ($k_B T \leq 0.3$ eV), however, this does not strongly influence the results. $\kappa(T)$ initially increases rapidly with T , but then reached a maximum followed by a rapid drop with T . This behavior differs qualitatively from the results for Nb. This difference is discussed extensively in the next section.

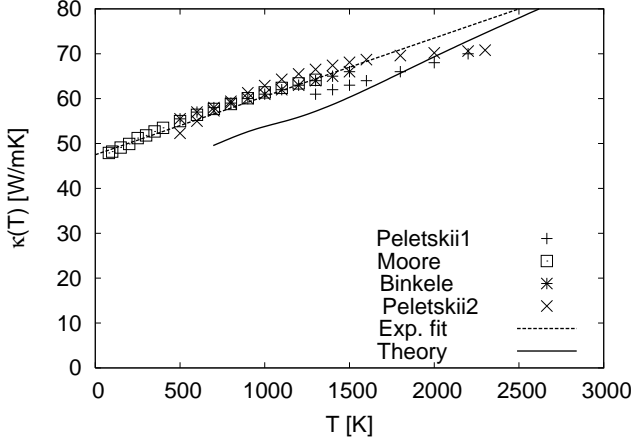


FIG. 2: Thermal conductivity of Nb metal according to the SC method (full line) and from experiments (“Peletskii1”¹⁶, “Moore”¹⁷, “Binkale”¹⁸, “Peletskii2”¹⁹) together with the line $\kappa(T) = 47.5 + 0.013T$ adjusted to the experimental results. The calculated result was obtained for a $10 \times 10 \times 10$ lattice using a Gaussian broadening with the FWHM of 0.06 eV. The results was averaged over 10 different random displacements of the atoms. The model of Nb described in Sec. II was used. The figure shows that theory and experiment agree rather well and that $\kappa(T)$ increases approximately linearly with T .

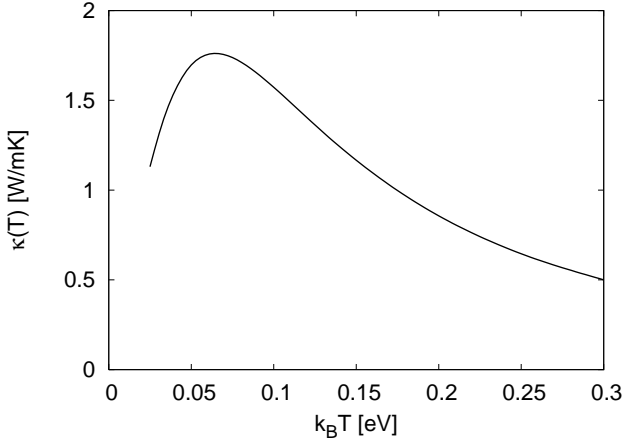


FIG. 3: Thermal conductivity of the C₆₀ model according to the SC method for $\lambda = 0.5$ and $\omega_{ph} = 0.1$ eV. 400 random configurations for a $8 \times 8 \times 8$ cluster were generated, and a Gaussian broadening of 0.03 eV FWHM was used.

VI. QUALITATIVE DISCUSSION IN SEMICLASSICAL FORMALISM

In this section we use the semiclassical formalism to discuss qualitatively both $T \ll W$ and $T \sim W$, where W is the band width. For this purpose we first derive a relation between matrix elements of the electrical and heat current operators. In the spirit of the semiclassical approximation, we assume noninteracting electrons.

Let $|l\rangle$ be a one-particle eigenstate with the energy ε_l .

Using the definition of \mathbf{j}_E in Eq. (9)

$$\begin{aligned} \langle l | \mathbf{j}_E | l' \rangle &= \frac{i}{\hbar} (\varepsilon_l - \varepsilon_{l'}) \sum_i \mathbf{R}_i \langle l | h_i | l' \rangle \\ &= \frac{i}{2\hbar} (\varepsilon_l - \varepsilon_{l'}) (\varepsilon_l + \varepsilon_{l'}) \sum_i \mathbf{R}_i \langle l | n_i | l' \rangle \\ &= \frac{1}{2} (\varepsilon_l + \varepsilon_{l'}) \langle l | \mathbf{j} | l' \rangle \end{aligned} \quad (21)$$

It then follows that

$$\langle l | \mathbf{j}_Q | l' \rangle = \left(\frac{\varepsilon_l + \varepsilon_{l'}}{2} - \mu \right) \langle l | \mathbf{j} | l' \rangle. \quad (22)$$

We now consider values of T which are sufficiently large to give a large thermal disorder. As a result there are matrix elements of the current operators between essentially all states. We therefore make the assumption that all the matrix elements of the particle current operator between different eigenstates of the Hamiltonian have the same value j_{av} . This assumption has been checked extensively and found to lead to accurate results for $\sigma(\omega)$ for large T .⁷ It is important to make this assumption for the particle current operator, since it would obviously not be true for the heat current operator, as can be seen from Eq. (22), due to the factor $[(\varepsilon + \varepsilon')/2 - \mu]$.

We first consider the case when $T \ll W$. We can assume that the density of states per orbital and spin, $N(\varepsilon)$, is a constant $N(\mu)$, since states close to $\varepsilon = \mu$ mainly influence $\text{Im } \pi^{nm}(\omega)$ for small ω and $T \ll W$. This gives

$$\begin{aligned} \text{Im} \pi_{xx}^{(22)}(\omega) &= -\frac{2\pi\hbar}{N\Omega} [N N_d N(\mu) j_{av}]^2 \\ &\times \int d\varepsilon d\varepsilon' \left(\frac{\varepsilon + \varepsilon'}{2} - \mu \right)^2 [f(\varepsilon) - f(\varepsilon')] \delta(\hbar\omega + \varepsilon - \varepsilon'). \end{aligned} \quad (23)$$

We now consider the limit $\omega \ll T$. We also use the assumption $T \ll W$ to extend the integrations in Eq. (23) to infinity. To leading order in ω we then obtain

$$\text{Im} \pi_{xx}^{(22)}(\omega) = -\frac{2\pi^3 (k_B T)^2}{3\Omega} N [N_d N(\mu) j_{av}]^2 \hbar^2 \omega. \quad (24)$$

Similar approximations lead to

$$\text{Im} \pi_{xx}^{(12)}(\omega) = 0 \quad (25)$$

and

$$\text{Im} \pi_{xx}^{(11)}(\omega) = -\frac{2\pi}{\Omega} N [N_d N(\mu) j_{av}]^2 \hbar^2 \omega. \quad (26)$$

From Eqs. (12,13) we then obtain

$$\frac{\kappa(0)}{\sigma(0)T} = \frac{\pi^2}{3} \left(\frac{k_B}{e} \right)^2, \quad (27)$$

which is the Wiedemann-Franz law.

To obtain further understanding, we make some more explicit estimates. We first derive a sum rule for the particle current matrix elements.

$$\sum_{l'l'\alpha} |j_{l'l',\alpha}|^2 = \left(\frac{d}{\hbar}\right)^2 \sum_{\mu\nu} |t_{\mu\nu}|^2 = \frac{NN_d d^2}{\hbar^2} \langle \varepsilon^2 \rangle, \quad (28)$$

where α labels a coordinate, d is the separation of two atoms and $\langle \varepsilon^2 \rangle$ is the second moment of the density of states per site, orbital and spin. On the left hand side, the states $|l\rangle$ refer to extended eigenstates. In the middle expression, we have made a unitary transformation to localized basis states and used Eq. (7), assuming nearest neighbor hopping only. Since the number of matrix elements on the left hand side of Eq. (28) is $3(NN_d)^2$, we obtain

$$|j_{av}|^2 = \frac{d^2}{3NN_d \hbar^2} \langle \varepsilon^2 \rangle. \quad (29)$$

Typically, $\langle \varepsilon^2 \rangle N(\mu)^2 \approx 0.1$ for a system close to half-filling.⁷ Inserting this in Eqs. (13, 24) we obtain

$$\kappa = \frac{0.2\pi^3}{9} \frac{d^2}{\hbar\Omega} N_d k_B^2 T = 0.9 N_d \frac{k_B^2 T}{\hbar d}, \quad (30)$$

where we have used that $\Omega/d^2 = (4/3\sqrt{3})d$, as appropriate for Nb metal with a bcc lattice. This gives the large T behavior $\kappa = 0.027T$ W/Km for Nb, where T is in K. This could be compared with the linear behavior fitted to experimental result¹⁵ $\kappa = (47.5 + 0.013T)$ W/Km (see Sec. V), where the linear term in T is about a factor of two smaller than our simple estimate.

Comparing the result in Eq. (30) with Eq. (1) we find that we have to assume that

$$l \approx 0.8 N_d^{1/3} d, \quad (31)$$

to obtain the estimated thermal conductivity. This is essentially the Ioffe-Regel condition.

We now discuss the reasons for the saturation of the mean free path and the linear increase of κ with T , using the semiclassical treatment of the phonons. At small T , there are important intraband transitions for small wave vectors \mathbf{q} , which make contributions to $\text{Im } \pi^{(22)}(\omega)$ for small ω . As T is increased, the increasing thermal disorder leads to a strong violation of momentum conservation (in the electronic system) and many transitions that were strongly suppressed at small T become important for large T . At the same time the transitions corresponding to small ω are reduced. However, the sum rule in Eq. (28) shows that the sum over all particle current matrix elements squared is not reduced, as long as the hopping integrals are not reduced. Thus even if we assume that the particle current matrix elements corresponding to low energy transitions are not larger than the average of the matrix elements, there is still an appreciable (and saturating) weight of the transitions corresponding to a small energy transfer in Eq. (23). The

prefactor $[(\varepsilon + \varepsilon')/2 - \mu]^2$ in Eq. (23) furthermore gives increasingly large contributions as T is increased and the Fermi functions are broadened. This leads to the increase in $\kappa(T)$ with T and it corresponds to the increase in the specific heat per electron with T entering in the Sommerfeld theory leading to Eq. (1).

We next consider the case when $T \sim W$. This is uninteresting for Nb, due to its large band width, but of relevance for A_3C_{60} for which the band width is small. In A_3C_{60} the phonons couple to the level energies. As a result the hopping integrals in Eq. (28) are not changed and j_{av} is unchanged as T is increased. On the other hand, due to the fluctuations of the level energies, the band width grows with T as⁷

$$W(T) = W(T=0) \sqrt{1 + c\lambda \frac{k_B T}{W(T=0)}}, \quad (32)$$

where c is of the order 15. Thus there are substantial effects on the band width already for $k_B T \sim W/10$. To describe these effects we assume that the density of states can be written as

$$N(\varepsilon, T) = \frac{1}{\sqrt{1 + T/T_0}} n\left(\frac{\varepsilon}{\sqrt{1 + T/T_0}}\right), \quad (33)$$

where $n(\varepsilon)$ is assumed to have no explicit T dependence and $k_B T_0 \approx 0.1$ eV. We have

$$\begin{aligned} \sigma(\omega) &= \frac{2\pi e^2 N}{\omega \Omega} (N_d j_{av})^2 \int d\varepsilon \int d\varepsilon' N(\varepsilon, T) N(\varepsilon', T) \\ &\quad \times [f(\varepsilon) - f(\varepsilon')] \delta(\hbar\omega + \varepsilon - \varepsilon'). \end{aligned} \quad (34)$$

In Ref. 7, a qualitative discussion of the electrical conductivity was given, neglecting finite T effects on the Fermi functions and emphasizing the difference between coupling to the level positions and hopping integrals. Thus the Fermi functions were replaced by Θ -functions. If this is done in Eq. (34) and j_{av} is assumed to be T independent, we obtain that $\sigma(0) \sim 1/(1 + T/T_0)$ and the integral over $\sigma(\omega)$, entering the f-sum rule, goes as $1/\sqrt{1 + T/T_0}$, in agreement with the results in Ref. 7. For the treatment of the thermal conductivity, however, it is crucial to include the T dependence of the Fermi functions. The ε' integration can trivially be performed, leading to a factor $f(\varepsilon) - f(\varepsilon + \hbar\omega)$. Assuming that $T \gg W$, we can approximate this factor as $\hbar\omega/(4k_B T)$. This gives

$$\begin{aligned} \sigma(\omega) &= \frac{\pi e^2 \hbar N}{2\Omega T \sqrt{1 + T/T_0}} (N_d j_{av})^2 \\ &\quad \times \int dx n(x) n\left(x + \frac{\hbar\omega}{\sqrt{1 + T/T_0}}\right) \\ &\equiv \frac{1}{(T/T_0) \sqrt{1 + T/T_0}} \tilde{g}\left(\frac{\hbar\omega}{\sqrt{1 + T/T_0}}\right), \end{aligned} \quad (35)$$

i.e., for very large T , $\sigma(0)$ decays as $T^{-3/2}$. Similar calculations for the thermal conductivity give

$$\kappa(\omega) = \frac{\pi \hbar N \sqrt{1 + T/T_0}}{2T^2} (N_d j_{av})^2$$

$$\begin{aligned} & \times \int dx n(x) n(x + \frac{\hbar\omega}{\sqrt{1+T/T_0}})(x + \frac{\hbar\omega}{2\sqrt{1+T/T_0}})^2 \\ & \equiv \frac{\sqrt{1+T/T_0}}{(T/T_0)^2} \tilde{h}(\frac{\hbar\omega}{\sqrt{1+T/T_0}}), \end{aligned} \quad (36)$$

As a result, the Wiedemann-Franz law is strongly violated and $\kappa(0)/\sigma(0) \sim \text{const}$ instead of T for very large T .

An important difference between $T \ll W$ and $T \gg W$ is the behavior of the specific heat. For a fixed band width and a small T , the energy of noninteracting electrons increases as T^2 due to the smearing out of the Fermi function. This leads to an increase in the specific heat per electron, $c_v \sim T$, as shown in Eq. (1), and results in $\kappa/\sigma \sim T$. For $T \gtrsim W$, however, the electrons are already rather evenly distributed over the band width, and an additional increase of T does not increase the total energy very much. The result is that c_v then decreases with T . For such large T the semiclassical theory is invalid, and it is not possible to express κ in terms of l and c_v . Nevertheless, it is suggestive that $\kappa/\sigma \sim T$ is violated, although the proper power of T is not predicted by these arguments.

To test the accuracy of these arguments, we define

$$h(\hbar\omega, T) = \frac{(T/T_0)^2}{\sqrt{1+T/T_0}} \kappa(\omega \sqrt{1+T/T_0}), \quad (37)$$

and introduce an equivalent definition for $g(\hbar\omega, T)$ in terms of $\sigma(\omega)$. These functions are shown in Fig. 4 for different values of T . If the approximations introduced above were exact, the curves calculated for different values of T would be identical. For the values of T shown in Fig. 4, this requirement is quite well fulfilled for $g(\omega, T)$ and less well fulfilled for $h(\omega, T)$. The main source of error is that the approximation for $f(\varepsilon) - f(\varepsilon + \hbar\omega)$ in Eq. (35) is only valid for $k_B T \gg W$, and Fig. 4 shows results for $k_B T \geq W/3$. Nevertheless, varying T by a factor of almost ten only leads to a variation of the maximum values of $h(\omega, T)$ by less than a factor of two, providing support for the analysis above.

VII. CONCLUSIONS

We have studied the electronic part κ of the thermal conductivity of metals, using two different methods. Accurate results are obtained by using a determinantal Quantum Monte-Carlo (QMC) method together with a maximum entropy method (MEM). As a much simpler approach we use a method where the phonons but not electrons are treated semiclassically (SC). We applied these methods to a model of A_3C_{60} ($A = K, Rb$) and showed that they give very similar results for $\kappa(\omega)$ over most of the energy range if the renormalization of the phonon frequency is treated in the same way in both methods. For very small values of ω , however, the SC method gives a downturn. This is probably due to an

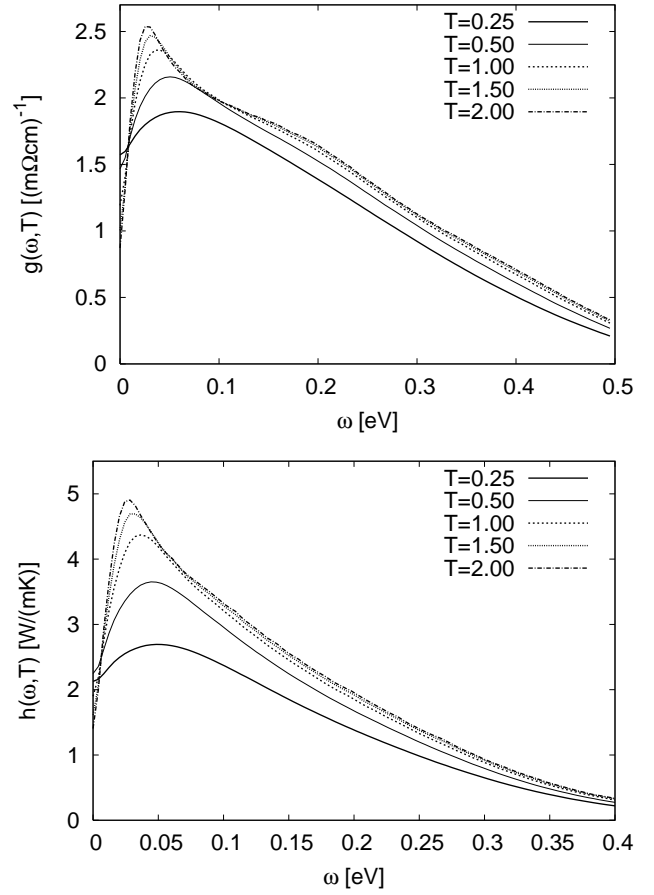


FIG. 4: Functions $g(\hbar\omega, T)$ and $h(\hbar\omega, T)$, defined in Eq. (37), as a function of ω for different values of $k_B T = 0.25, 0.5, 1.0, 1.5$ and 2.0 eV calculated using the SC method. The parameters are $\lambda = 0.5$ and $\omega_{ph} = 0.1$ eV. 400 random configurations for a $8 \times 8 \times 8$ cluster were generated, and a Gaussian broadening of 0.03 eV FWHM was used. If the approximations behind Eqs. (35,36) were exact, the curves would fall on top of each other.

incipient Anderson localization transition and a defect of the SC method neglecting that the scattering processes are inelastic. Applying the SC method to a model of Nb metal, we find that the results agree well with experiment. In particular, we find that $\kappa(T)$ increases with T , consistent with a saturation of the mean free path. In contrast, for A_3C_{60} at very large T , we find a decrease of $\kappa(T)$ with T . The results are analyzed in the SC method. To discuss very large T we use an approximation where all matrix elements of the electric current operator are assumed to be the equal. We can then qualitatively reproduced the calculated results for Nb, and give a quantum mechanical understanding of why the apparent mean free path saturates. Within this framework it is also possible to derive the Wiedemann-Franz law by assuming that $T \ll W$, where W is the band width. Due to the small band width of A_3C_{60} , we instead focus on the case $T \gtrsim W$ for this system. We then find that $\kappa(T) \sim T^{-3/2}$

indeed decreases with T and that the Wiedemann-Franz law is qualitatively violated.

-
- ¹ N. V. Ashcroft and N. D. Mermin, *Solid State Physics* (Holt, Rinehart and Winston, New York, 1976).
 - ² H. Wiesmann, M. Gurvitch, H. Lutz, A. Ghosh, B. Schwartz, M. Strongin, P.B. Allen, and J.W. Halley, Phys. Rev. Lett. **38**, 782 (1977).
 - ³ P. B. Allen, in *Superconductivity in d- and f-Band Metals* H. Suhl and M.B. Maple, Eds. (Academic, New York, 1980); in *Physics of Transition Metals*, P. Rhodes, Ed. (Inst. Phys. Conf. Ser. No. 55, 1980) p. 425.
 - ⁴ A. F. Ioffe and A. R. Regel, Prog. Semicond. **4**, 237 (1960).
 - ⁵ O. Gunnarsson, M. Calandra, and J.E. Han, Rev. Mod. Phys. **75**, 1085 (2003).
 - ⁶ M. Calandra and O. Gunnarsson, Phys. Rev. Lett. **87**, 266601 (2001).
 - ⁷ M. Calandra and O. Gunnarsson, Phys. Rev. B **66**, 205105 (2002).
 - ⁸ E.L. Wolf, *Principles of electron tunnelling spectroscopy* (Oxford University Press, New York, 1985) p. 268.
 - ⁹ O. Gunnarsson, *Alkali-doped Fullerenes - Narrow-band solids with unusual properties*, (World Scientific, Singapore, 2004).
 - ¹⁰ G. D. Mahan, *Many-Particle Physics*, (Plenum, New York, 1990), p. 651.
 - ¹¹ R. Blankenbecler, D.J. Scalapino, R.L. Sugar, Phys. Rev. D **24**, 2278 (1981).
 - ¹² M. Jarrell and J.E. Gubernatis, Phys. Rep. **269**, 133 (1996).
 - ¹³ J. E. Hirsch, Phys. Rev. B **31**, 4403 (1985).
 - ¹⁴ P.A. Lee and T.V. Ramakrishnan, Rev. Mod. Phys. **57**, 287 (1985).
 - ¹⁵ K. G. White, in *Landolt-Börnstein: Numerical data and functional relationships in science and technology*, New Series III/15c, edited by O. Madelung and K.G. White, (Springer, Berlin, 1991).
 - ¹⁶ V. E. Peletskii, Rev. Int. Hautes Temp. Refract. **12**, 90 (1975).
 - ¹⁷ J. P. Moore, R. S. Graves, and R. K. Williams, High. Temp. - High Pressures **12**, 579 (1980).
 - ¹⁸ L. Binkle, High. Temp. - High Pressures **18**, 599 (1986).
 - ¹⁹ V. E. Peletskii, A. P. Grishchuk, E. B. Zaretskii, A. A. Zolotukhin, Teplofiz. Vys Temp. **25**, 285 (1987); High Temp. (English Transl.) **25**, 205 (1987).